Lead Iron Oxides

DOI: 10.1002/ange.200602480

Crystallographic Shear Structures as a Route to Anion-Deficient Perovskites**

Artem M. Abakumov, Joke Hadermann, Sara Bals, Ivan V. Nikolaev, Evgeny V. Antipov, and Gustaaf Van Tendeloo*

Because of the technological importance of perovskite-based oxides, numerous pathways towards new structures have been developed, including ordering at the A and/or B cation sites of the perovskite (ABO_3) structure, vacancy ordering at the anion site, the intergrowth of perovskite and related structures, and the formation of hexagonal perovskite polytypes. However, it has been generally accepted that crystallographic shear (CS) structures cannot be realized in perovskites.[1] CS planes commonly occur in anion-deficient oxides derived from the ReO_3 or rutile (TiO_2) structures, which are based on metal-centered octahedra. Arrangement of the CS planes at different periodicities generates a homologous series. Some of the well-known examples of CS structures are M_nO_{3n-1}, M_nO_{3n-2} (M = Mo, W), Ti_nO_{2n-1}, and the block structures of Nb_2O_5 and its Ti-containing derivatives.[2–6] The shear operation is such that along the CS plane the octahedra share edges or faces, instead of corners or edges as in the basic structure. The ReO_3 structure is based on the same three-dimensional framework of corner-sharing BO_6 octahedra found in the perovskite structure, but the 12-coordinate A cation sites of the perovskite structure are empty in ReO_3. Usually, the presence of A cations in perovskites favors point defects in the anion sites (in a random or ordered arrangement), leading to a lower coordination number for the B cations, and prevents the elimination of anion point defects by a shear operation.[2] Herein, we report the occurrence of CS structures in perovskite-based "$Pb_2Fe_2O_5$" for the first time. We also describe the general crystallographic mechanism of CS-plane formation in a perovskite framework with the A sites filled by cations bearing a lone $6s^2$ electron pair, which involves the elimination of O vacancies by the shear operation and the relaxation of the structure at the CS plane. We discuss the role of the lone electron pair in directing structure formation, as well as the relationship between the crystallographic orientation of the CS plane and the chemical composition. The discovery of this mechanism opens up new possibilities for the design of novel perovskite-based compounds containing A cations with a lone $6s^2$ electron pair.

"$Pb_2Fe_2O_5$" (or "$PbFeO_{2.5}$") is expected to be an anion-deficient perovskite of the brownmillerite (Ca_2AlFeO_5) type;[7–9] however, its structure has not yet been determined. Because of the complexity of the structure and the prevalence of domain fragmentation, the only road to solving the structure is by transmission electron microscopy (TEM). The brighter reflections in the electron diffraction (ED) patterns of "$Pb_2Fe_2O_5$" (Figure 1a) reveal a perovskite sublattice with a parameter $a_p \approx 3.9$ Å (p denotes the perovskite subcell). Linear arrays of satellite reflections associated with each basic reciprocal lattice node are typical for periodic CS planes. The displacement vector for the CS planes was deduced from the ED patterns as $\mathbf{R} = 1/2\,[110]_p + 1/3\,[001]_p$ by measuring the fractional shifts $\mathbf{hR}$ for the satellite reflections (Figure 1b).[10,11][+] Closer inspection of the [010]*

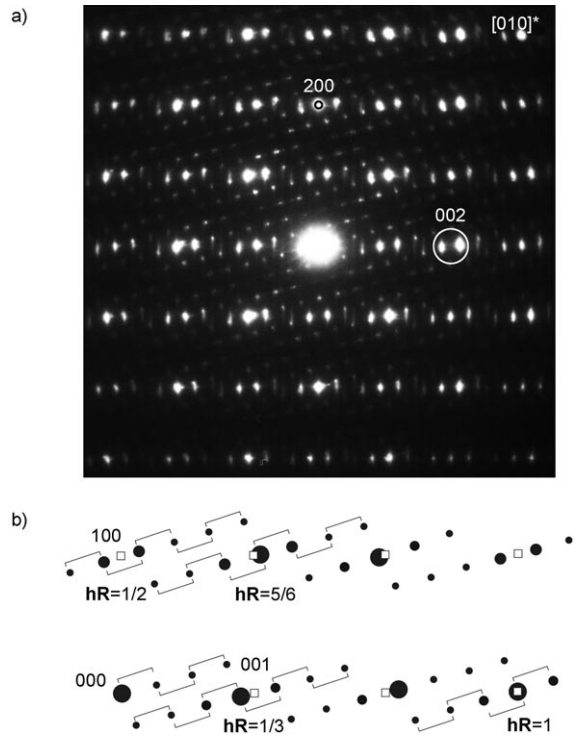

Figure 1. a) [010]* ED pattern of "$Pb_2Fe_2O_5$", indexed in the perovskite subcell. b) Derivation of fractional shifts $\mathbf{hR}$; empty squares indicate the positions of reciprocal lattice nodes of the perovskite subcell; square brackets denote the modulation vector $\boldsymbol{q}$; see text for details.

[*] Dr. A. M. Abakumov, I. V. Nikolaev, Prof. E. V. Antipov
Department of Chemistry
Moscow State University
119992 Moscow (Russia)
Fax: (+7) 495-939-47-88
E-mail: abakumov@icr.chem.msu.ru
Prof. J. Hadermann, Dr. S. Bals, Prof. G. Van Tendeloo
Centre for Electron Microscopy for Materials Science
University of Antwerp
Groenenborgerlaan 171, 2020 Antwerp (Belgium)

[**] The work was supported in part by the IAP V-1 program of the Belgium government and by the Russian Foundation for Basic Research (RFBR; 05-03-34812, 06-03-90168). The authors acknowledge Pavel S. Chizhov for the ELF calculations. S.B. is grateful to the Fund for Scientific Research, Flanders.

[+] The fractional-shift method describes the positions of the satellite reflections as $\mathbf{H} = \mathbf{h} + [m + \mathbf{hR}]\,\boldsymbol{q}$, where $\mathbf{H}$ and $\mathbf{h}$ are satellite and basic diffraction vectors, $\boldsymbol{q}$ is the modulation vector, m is the order of the satellite reflection, and $\mathbf{R}$ is the displacement vector of the CS planes. The product $\mathbf{hR}$ results in the fractional shift of the array of satellites with respect to the position of the basic reflection.

ED pattern reveals the incommensurate character of the modulation. The monoclinic unit-cell parameters (denoted by m) for the commensurate approximant are $\mathbf{a}_m = 3\mathbf{a}_p + 7\mathbf{c}_p$, $\mathbf{b}_m = \mathbf{b}_p$, $\mathbf{c}_m = -4\mathbf{a}_p + \mathbf{c}_p$ ($a_m = 29.881$, $b_m = 3.884$, $c_m = 16.062$ Å, $\beta = 98.49°$; space group $C2/m$). The CS planes are parallel to $(100)_m = (104)_p$.

The cation positions in "$Pb_2Fe_2O_5$" were determined using high-angle annular dark field (HAADF) scanning transmission electron microscopy (STEM). In the scanning transmission mode, the intensity related to a column of atoms is proportional to Z^n ($1 < n < 2$), where Z is the average atomic number of the projected column. This relationship often allows a straightforward interpretation of HAADF STEM images. The brighter spots on the unfiltered [010] HAADF STEM image of "$Pb_2Fe_2O_5$" (Figure 2a) are associated with the Pb columns, whereas the weaker spots (difficult to see in Figure 2a) correspond to the projection of the Fe columns. The resulting atomic arrangement of the cations is shown in Figure 2b. The perovskite blocks (outlined by thick dashed lines in Figure 2b) have a length of $4a_p$ and are mutually shifted along c_p by one perovskite unit cell, according to the $(104)_p$ orientation of the CS plane. Between the perovskite blocks, six-sided channels consisting of six Fe columns surrounding two Pb columns are formed (outlined by thin solid lines in Figure 2b). This arrangement is confirmed by simulations of the [010] HAADF STEM image (Figure 2a).

The new structure is derived from the perovskite structure by a periodic insertion of $(104)_p$ CS planes with the displacement vector $\mathbf{R} = \mathbf{R}_0 + \mathbf{R}_1$, where $\mathbf{R}_0 = 1/2[110]_p$ and $\mathbf{R}_1 = 1/3[001]_p$. The $\mathbf{R}_0$ shift applied along the $(\bar{1}01)_p$ plane eliminates the O atoms marked as open squares in Figure 3a. The O atoms at the edges of the perovskite unit cell parallel to c_p (gray square in Figure 3a) are not eliminated by the shear operation, but cannot be retained together with the Pb columns, owing to abnormally short Pb–O separations. The $\mathbf{R}_0$ displacement introduces columns of edge-sharing FeO_5 square pyramids that are bridged through corner sharing with columns of FeO_6 octahedra (Figure 3b). Pb atoms are positioned inside the resulting channels, where space is available for their lone $6s^2$ electron pairs. However, the $\mathbf{R}_0$ shear alone would lead to very short Pb–Pb separations of $a_p/\sqrt{2} \approx 2.76$ Å between the Pb atoms within the channels. The displacement $\mathbf{R}_1$ increases this distance to 3.56 Å (Figure 3c). The $\mathbf{R}_1$ displacement also distorts the FeO_5 square pyramids, making the coordination environment of the Fe atoms closer to a trigonal bipyramid.

CS planes with high $(h0l)$ indices can be considered as composed of short segments of low-index CS planes, such as the $(\bar{1}01)_p$ and $(001)_p$ planes, as the main constituents. The $1/2[110]_p(\bar{1}01)_p$ structure (in which square brackets indicate the displacement vector and parentheses indicate the orientation of the CS plane) contains layers of six-sided channels parallel to $(\bar{1}01)_p$ (Figure 3d), which are separated by n perovskite layers, resulting in a $A_2Fe_2O_4 + n\,AFeO_3$ homologous series.

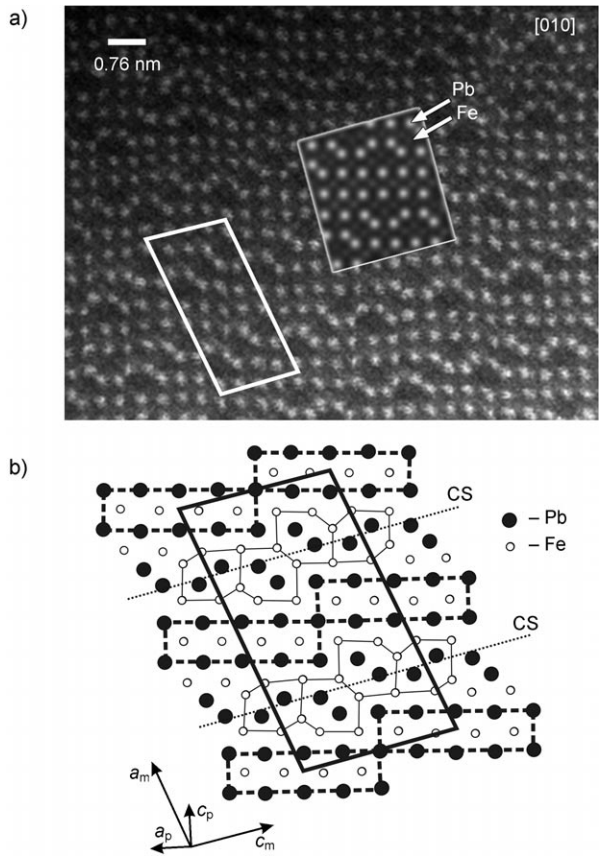

Figure 2. a) [010] HAADF STEM image of "$Pb_2Fe_2O_5$"; the monoclinic unit cell is outlined by thick white lines; a simulation of the image is outlined by thin white lines. b) Arrangement of the columns of Pb and Fe atoms in "$Pb_2Fe_2O_5$"; the monoclinic unit cell is outlined by thick solid lines; the perovskite blocks are outlined by thick dashed lines; the six-sided channels are outlined by thin solid lines; the CS planes are indicated by thin dotted lines.

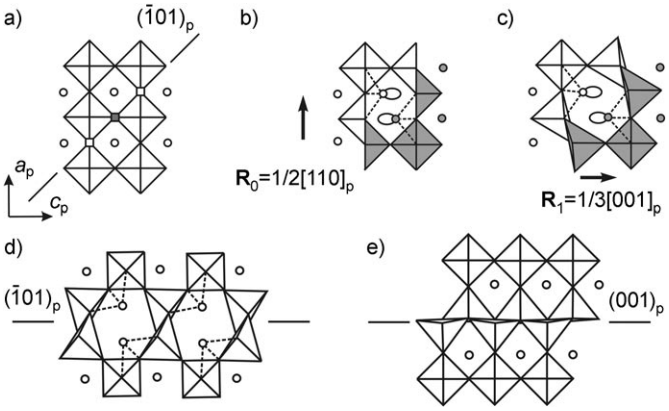

Figure 3. Generation of CS planes in "$Pb_2Fe_2O_5$": a) creation of O vacancies (squares) along the $(\bar{1}01)_p$ plane; b) application of the $\mathbf{R}_0 = 1/2[110]_p$ displacement vector, leading to the formation of FeO_5 square pyramids and six-sided channels; c) application of the $\mathbf{R}_1 = 1/3[001]_p$ displacement vector, leading to an increase in the Pb–Pb separation within the channels; circles Pb (with lone $6s^2$ electron pairs), polyhedra FeO_6/FeO_5; displaced part of the structure is gray. d) Structure of the low-index $1/2[110]_p(\bar{1}01)_p$ CS plane. e) Structure of the low-index $1/2[110]_p(001)_p$ CS plane.

Despite not having been previously considered as a CS structure, $Pb_{1.33}Sr_{0.67}Fe_2O_5$ ($A_4Fe_4O_{10}$) corresponds to the second member ($n=2$) of this series.[12]

The $1/2[110]_p(001)_p$ operation could be a conservative shear, since the displacement vector is parallel to the interface plane. However, the $1/2[110]_p$ shift along the FeO_2 plane transforms the FeO_6 octahedra into twice as many FeO_5 square pyramids (Figure 3e). Only half of the square pyramidal sites are occupied by Fe atoms; however, filling the vacant sites by extra Fe atoms would result in a composition of Fe_2O_2 for the layer and an excess of Fe with respect to the overall composition. These double layers of edge-sharing FeO_5 pyramids can be separated by perovskite layers, leading to $AFe_2O_3 + n\,AFeO_3$ homologues. Similar alternating double layers of strongly distorted FeO_5 pyramids and perovskite layers of FeO_6 octahedra occur in $Sr_4Fe_6O_{12+\delta}$ ($A_2Fe_3O_6$), which can be considered as the $n=1$ member of the homologous series.[13]

The $1/2[110]_p(104)_p$ CS structure observed for "$Pb_2Fe_2O_5$" can be broken up as $2(101)_p + (\bar{1}01)_p + (001)_p$, resulting in a composition of $3\,Pb_2Fe_2O_4 + PbFe_2O_3 + 8\,PbFeO_3 = Pb_{15}Fe_{16}O_{39}$, since the perpendicular $(101)_p$ and $(\bar{1}01)_p$ planes delimit rectangular perovskite blocks of eight FeO_6 octahedra.

Other CS planes, such as $(\bar{3}05)_p$, were also observed for "$Pb_2Fe_2O_5$" (in the same sample). The corresponding CS structure can be represented as $3(\bar{1}01) + 2(001)$ with a composition of $3\,Pb_2Fe_2O_4 + 2\,PbFe_2O_3 + 10\,PbFeO_3 = Pb_{18}Fe_{20}O_{48}$, because the perovskite layers between the CS planes have an average thickness of two FeO_6 octahedra. The cation composition agrees with the Pb deficiency experimentally determined using energy-dispersive X-ray (EDX) microanalysis (Pb:Fe = 0.90(3):1.00).

The [010] projections of the $Pb_{15}Fe_{16}O_{39}$ and $Pb_{18}Fe_{20}O_{48}$ structures are shown in Figure 4; experimental evidence for the structures is presented in Figure 5. Image simulations based on the structures in Figure 4 (Figure 5, insets) are in excellent agreement with the experimental high resolution electron microscopy (HREM) images.

The CS structures in "$Pb_2Fe_2O_5$" ($1/2[110]_p(\bar{1}04)_p$ and $1/2[110]_p(\bar{3}05)_p$ CS planes), $Pb_{1.33}Sr_{0.67}Fe_2O_5$ ($1/2[110]_p(\bar{1}01)_p$ CS plane),[12] and $PbMnO_{2.75}$ ($1/2[110]_p(704)_p$ CS plane)[14] occur because the B cations are able to adopt coordination numbers of 5 or 6 and because the Pb^{2+} cations, which have a lone electron pair, favor an asymmetric coordination environment. The Pb atoms within the six-sided channels of all three structures are coordinated to O atoms at three short (2.28–2.43 Å) and three long (2.63–2.70 Å) Pb–O distances.[12] The lone $6s^2$ electron pair E completes the coordination polyhedron of the Pb atoms (PbO_6E). We confirmed the localization of the lone electron pairs on the Pb atoms in the six-sided channels by analyzing the electron localization function (ELF) distribution in the $Pb_{1.33}Sr_{0.67}Fe_2O_5$ structure. Typically ionic cations, such as Sr^{2+} prefer the A sites in the perovskite blocks. This result agrees with the experimentally observed Pb and Sr distribution in $Pb_{1.33}Sr_{0.67}Fe_2O_5$, in which the six-sided channels are exclusively filled with Pb^{2+} cations.[12]

It is expected that the building principles derived herein can lead to new perovskite-based compounds, in which the chemical composition is adjusted by varying the orientation of the CS plane and the thickness of the separating perovskite slabs. In the CS structures observed herein, the size of the perovskite slabs between CS planes of a particular orientation is determined by the oxidation state of the Fe cations; thus, a change in the partial O_2 pressure or the synthesis temperature could induce a variety of other possible structures. The power of the new structural principles becomes clear if one considers introducing two types of B cations with different oxidation states and coordination numbers, in addition to an A cation with a lone electron pair, into the perovskite-based structure.

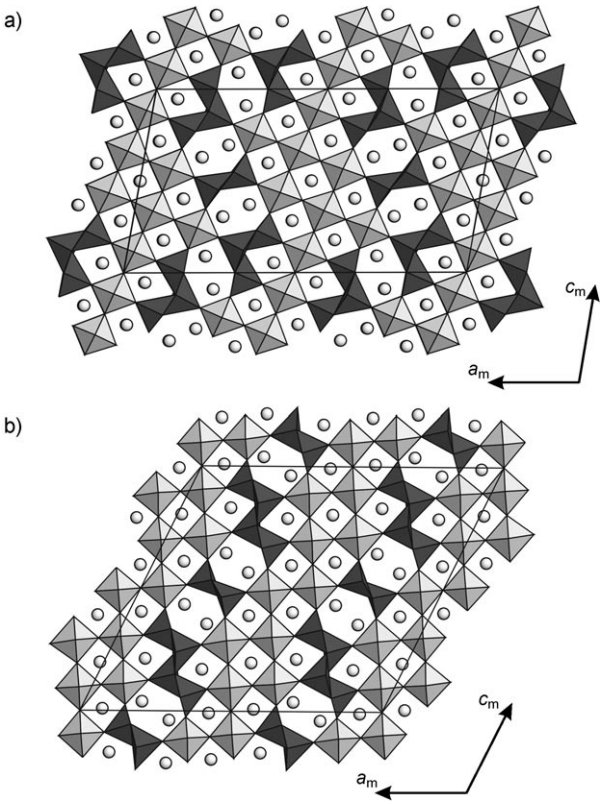

Figure 4. [010] projections of the a) $Pb_{15}Fe_{16}O_{39}$ and b) $Pb_{18}Fe_{20}O_{48}$ CS structures; circles Pb, gray polyhedra FeO_6, black polyhedra FeO_5.

Experimental Section

"$Pb_2Fe_2O_5$" was prepared by annealing PbO and Fe_2O_3 in a 2:1 ratio in air at 800 °C for 210 h. The X-ray diffraction pattern of the product was fit using the Le Bail method, resulting in the parameters $a=3.8879(2)$, $b=3.8838(2)$, $c=3.9386(3)$ Å, $\beta=90.291(6)°$, $\mathbf{q}=0.03760(1)\mathbf{a}^*+0.12981(2)\mathbf{c}^*$ ($\mathbf{q}=1/2\,\boldsymbol{q}$, where $\boldsymbol{q}$ is the modulation vector used for the fractional-shift method) and the (3+1)D space group $X2/m(\alpha 0\gamma)$, $X=[1/2,\ 1/2,\ 1/2,\ 1/2]$. The EDX analysis was performed on a JEOL JSM 5510 electron microscope with an INCA attachment. For the electron microscopy, Philips CM20, Jeol 4000EX, and Jeol 3000F instruments were used. Image simulations were carried out with the MacTempas software. The ELF distribution was evaluated for a model compound of composition $PbSrFe_2O_5$, in which the mixed-occupancy ($Pb_{0.33}Sr_{0.67}$) position in the perovskite block of the $Pb_{1.33}Sr_{0.67}Fe_2O_5$ structure is fully occupied by Sr. The ELF was determined from the results of density functional theory (DFT) calculations performed using the TB-LMTO-ASA method and the

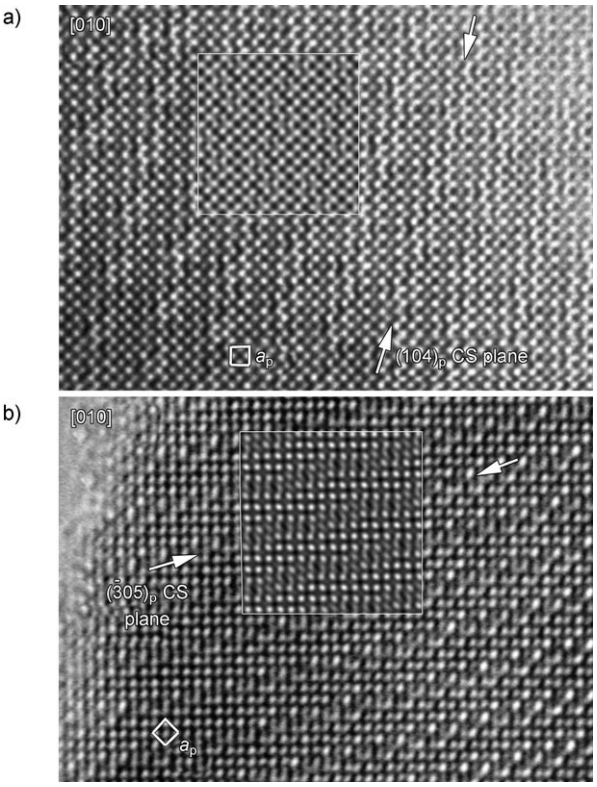

Figure 5. [010] HREM images of the a) $Pb_{15}Fe_{16}O_{39}$ $(1/2[110]_p(104)_p$ CS plane) and b) $Pb_{18}Fe_{20}O_{48}$ $(1/2[110]_p(\bar{3}05)_p$ CS plane) structures; the cubic perovskite unit cell is outlined by thick white lines; simulations of the images ($\Delta f = -275$ Å, $t = 30$ Å (a); $\Delta f = -200$ Å, $t = 30$ Å (b) are outlined by thin white lines. Δf = defocus, t = thickness.

Barth–Hedin exchange-correlation potential,[15] with the LMTO 4.7 program package.[16]

Received: June 20, 2006
Published online: September 13, 2006

Keywords: crystallographic shear · electron microscopy · iron · lead · perovskite phases

[1] R. H. Mitchell, *Perovskites: Modern and Ancient*, Almaz Press, Thunder Bay (Canada), **2002**.
[2] A. Magneli, *Acta Chem. Scand.* **1948**, *2*, 501 – 517.
[3] L. Kihlborg, *Ark. Kemi* **1963**, *21*, 443 – 460.
[4] A. D. Wadsley, *Rev. Pure Appl. Chem.* **1955**, *5*, 165 – 193.
[5] S. Andersson, L. Jahnberg, *Ark. Kemi* **1963**, *21*, 413 – 426.
[6] A. D. Wadsley, *Acta Crystallogr.* **1961**, *14*, 660 – 664; A. D. Wadsley, *Acta Crystallogr.* **1961**, *14*, 664 – 670.
[7] J.-C. Grenier, M. Pouchard, P. Hagenmuller, *Rev. Chim. Miner.* **1977**, *14*, 515 – 522.
[8] J. Mexmain, S.-L. Hivert, *Ann. Chim.* **1978**, *3*, 91 – 97.
[9] F. P. Glasser, *Am. Mineral.* **1967**, *52*, 1085 – 1093.
[10] J. Van Landuyt, R. De Ridder, R. Gevers, S. Amelinckx, *Mater. Res. Bull.* **1970**, *5*, 353 – 362.
[11] D. Van Dyck, D. Broddin, J. Mahy, S. Amelinckx, *Phys. Status Solidi A* **1987**, *103*, 357 – 373.
[12] V. Raynova-Schwarten, W. Massa, D. Z. Babel, *Z. Anorg. Allg. Chem.* **1997**, *623*, 1048 – 1054.
[13] M. D. Rossell, A. M. Abakumov, G. Van Tendeloo, J. A. Pardo, J. Santiso, *Chem. Mater.* **2004**, *16*, 2578 – 2584.
[14] C. Bougerol, M. F. Gorius, I. E. Grey, *J. Solid State Chem.* **2002**, *169*, 131 – 138.
[15] U. Barth, L. Hedin, *J. Phys. C* **1972**, *5*, 1629 – 1642.
[16] O. Jepsen, A. Burkhardt, O. K. Andersen, *The TB-LMTO-ASA Program*, Version 4.7, Max-Planck-Institut für Festkörperforschung, Stuttgart (Germany), **1999**.

